PCCP

Accepted Manuscript

This is an *Accepted Manuscript*, which has been through the Royal Society of Chemistry peer review process and has been accepted for publication.

Accepted Manuscripts are published online shortly after acceptance, before technical editing, formatting and proof reading. Using this free service, authors can make their results available to the community, in citable form, before we publish the edited article. We will replace this *Accepted Manuscript* with the edited and formatted *Advance Article* as soon as it is available.

You can find more information about *Accepted Manuscripts* in the Information for Authors.

ROYAL SOCIETY OF CHEMISTRY

www.rsc.org/pccp

PAPER space-1cm www.rsc.org/faraday_d | Faraday Discussions

Tailoring the Optical Gap of Silicon Quantum Dots without Changing Their Size[†]

Huashan Li,[a] Zhigang Wu,[b] Tianlei Zhou,[c] Alan Sellinger,[c] and Mark T. Lusk[d]

**The absorption of photons through the direct generation of spatially separated excitons at dot-ligand interfaces is proposed as a promising strategy for tailoring the optical gap of small silicon quantum dots independent of their size. This removes a primary drawback for the use of very small dots in broad range of applications. For instance, the strategy can be applied to solar energy technologies to align the absorption of such dots with the peak of the solar spectrum. The key is to establish both a Type-II energy level alignment and a strong electronic coupling between the dot and ligand. Our first principles analysis indicates that connecting conjugated organic ligands to silicon quantum dots using vinyl connectivity can satisfy both requirements. For a prototype assembly of 2.6 nm dots, we predict that triphenylamine termination will result in a 0.47 eV redshift along with an enhanced near-edge absorption character. Robustness analyses of the influence of oxidation on absorption and of extra alkyl ligands reveal that the control of both factors is important in practical applications.**

Introduction

Colloidal semiconductor quantum dots (QDs) have received significant attention for applications in light emission,[1] optical computing,[2] photovoltaics,[3] and biomedical imaging, sensing and treatments[4–6] because of their unique properties. These include tunable absorption and emission spectra, solution processability, multiple exciton generation,[7] and slow cooling rate of hot carriers.[8] Most of the QDs currently ex-

plored, though, are based on metal chalcogenide semiconductors that use toxic elements such as cadmium and/or lead—a severe drawback for the applications described above.[9] In contrast, recent achievements in the synthesis, processing and purification of environmentally benign silicon-based quantum dots (SiQDs) make their use much more promising going forward.[10]
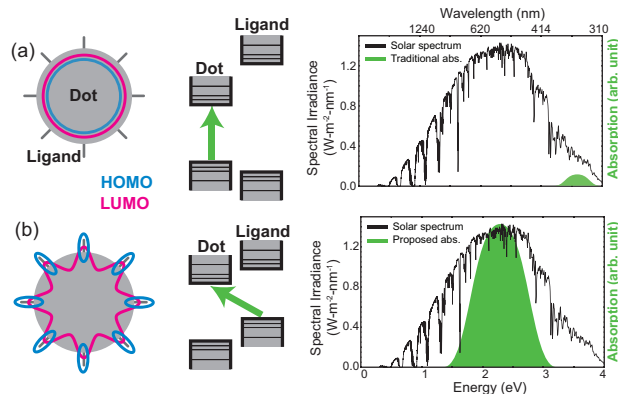
Fig. 1 Schematics of (a) traditional passivation schemes with a Type-I energy level alignment between the dot and the ligand, and a Si-C-C connection; and (b) our proposed scheme with a Type-II interface and a Si-C=C conjugating connection. The blue and pink solid lines indicate the highest occupied molecular orbital (HOMO) and lowest unoccupied molecular orbital (LUMO) localization, respectively. The corresponding energy level alignment in each case is illustrated in the middle of each panel, and the green arrows notify the transitions associated with the low-energy absorption. For each situation, the absorption spectrum is scratched on the right to illustrate the match to the solar spectrum (Air Mass 1.5 from the website of American Society for Testing and Materials).

However, there are challenges associated with a silicon-based paradigm as well: dangling bond defects tend have a deleterious effect on the optical performance of silicon quantum dots (SiQDs);[11] the dots tend to agglomerate in solution; assemblies of SiQDs have extremely poor carrier mobility;[12] and dot designs must contend with the fact that the band edge absorption of bulk silicon is low because of its indirect character. Within the setting of solar energy harvesting, SiQD-based

photovoltaic (PV) devices that have been created as hybrid SiQD/organic polymer blends [11,13–15] and SiQD/bulk heterojunction tandem solar cells [16–18] have efficiencies that are quite low [9].

Many of these issues can be addressed by focusing on small SiQDs. Dangling bond defects can be essentially eliminated by making the dots sufficiently small, [19] and the absorption cross-section of sufficiently small dots is dramatically enhanced via a pseudo-direct optical transition. [20–22] These call for SiQDs on the order of 1-4 nm. [23] This size regime has other advantages as well. SiQDs of this size transport excitons more efficiently [21] resist oxidation better, [23] use their slice of the solar spectrum more efficiently [24], show greater promise in multiple-exciton generation and hot carrier collection paradigms, [25] and have a higher excitonic coupling for the same surface-to-surface separation. [21]

Unfortunately, SiQDs of this size have optical gaps in the range of 2-3 eV (600-400 nm)—poorly matched to the solar spectrum [26] and missing the important low-optical and IR regions for light emission applications. In addition, the associated exciton binding energies are too high to result in room temperature dissociation of charge carriers for photo-electric applications. Because of their high surface-to-volume ratio, though, it may be possible to functionalize their surfaces so as to remedy these drawbacks. Surface functionalization might also be used to improve carrier mobility and processability.

Capping of SiQDs is most commonly in the form of alkyl chains that help with solubility and protect against oxidation. [10,27] This results in a Type-I energy level alignment between the dot and the ligand with a large band offset, wherein both the HOMO and the LUMO are localized inside the core of the dot. Photon energies on the order of 3 eV are then required to produce excitons in the smallest SiQDs. A number of other capping groups have been considered, though, such as diols and epoxides [28], amine-terminated alkyls [29], and conjugating vinyl (Si-C=C) connections [21,30–32]. The resulting mixing of dot and ligand orbitals can induce a substantial increase in the oscillator strength.

In some instances, there has also been a report of a redshift in absorption and emission spectra [21,28–32], but these may well originate from the creation of new surface states, the change of dot energy levels due to surface treatment, and the transition between ligand and dot orbitals [21]. This is further complicated by the substantial impact of surface defects on absorption and emission spectra. In fact, the inevitable oxidation, in form of Si-O-Si, Si-OH, and Si=O structures, may cause both redshifts and blueshifts of SiQD spectra with depending on dot size and oxidation level. [23,33–36] Moreover, the dot synthesis technique employed in some cases results in structures that have yet to be fully characterized. [37] These issues motivated Atkins *et al.* to carry out a femtosecond transient absorption experiment in which the aminopropenyl-terminated

SiQDs show photoexcited carrier dynamics between the QDs and ligand—strong evidence for the existence of the charge transfer states [30]. However, their SiQDs were synthesized in aqueous solution, and even mild oxidation would change the localization of the wave function causing a noticeable redshift of the spectra. [21,29] Furthermore, it is not clear how the aqueous solvents with high dielectric constants contribute to the distinct characteristics of SiQDs with various passivations [38]. In general, the Type-I energy level alignment still sets the lower bound of the optical gap which is close to that of the hydrogen-passivated dot.

To help clarify the origin of the redshift and to help design passivation schemes to facilitate better absorption, ab initio simulations have been applied to SiQDs with various terminations [39–42]. Consistent with experiments, their results suggest that alkene and alkyne chains change the optical gap only slightly [39–41] while indicating that a low-level oxidation could cause noticeable redshift in spectra [43–45]. Interestingly, it was found that the HOMO and LUMO of passivated SiQDs can be localized on the ligand and dot, respectively, for dots with diameters $d \leq 1.5$ nm [41,42,46].

In contrast to these studies of involving common terminating groups, our efforts have focused on an explicit design strategy to enable the direct generation of spatially separated excitons at the interface between the core of the dot and its surface ligands (Fig. 1). As long as the coupling between the core and the terminating shell is sufficiently large, photons with energies much lower than the intrinsic band gaps of both the dot and the ligand can be absorbed to excite electrons from the HOMO, localized on the ligands, to the LUMO localized on the dot. In fact, this concept has been successfully applied to the core/shell nanocrystals. In that setting, Type-II architectures exhibit new absorption features in the range below the core energy gap as well as much lower charge recombination rates compared to their Type-I counterparts. [47–49]

The ability to generate partially separated excitons at Type-II interfaces suggests a new means of tailoring the optical gap associated with the HOMO of the ligand and the LUMO of the dot. To be useful, though, such capping must also result in large optical transition matrix elements between the unoccupied orbitals localized on the dot and the occupied orbitals localized on the ligand, endowing the system with a high absorption cross-section. Small, functionalized dots meeting both requirements would better match the solar spectrum while supporting strong absorption near the absorption edge. This has motivated our computational investigation to design a practical passivation strategy for SiQD assemblies that are promising for improving optical absorption and large-scale manufacturing. We demonstrate that meeting two conditions is sufficient to result in materials with efficient light harvesting based on spatially separated excitons:

- a Type-II energy level alignment

- conjugating vinyl bond (Si-C=C) connection between ligands and SiQDs

Computational Methods

All electronic structure calculations were carried out using density functional theory (DFT) within the generalized gradient approximation (GGA) for exchange and correlation as parameterized by Perdew, Burke, and Ernzerhof.[50] For passivated dots with $d < 2$ nm (Si_{211}), the structures were restricted to the D_2 symmetry and relaxed until all atomic forces were less than 0.002 Ha/Å. For dots with diameters greater than 2 nm, we have found that the geometry optimization from the bulk structures has negligible impact on electronic structures. Thus only the interface configurations were relaxed.

The ΔSCF method was employed to obtain quasi-particle HOMO and LUMO energy levels. For dots with $d < 20.5$ Å ($Si_{275}H_{172}$), an all-electron approach implemented in the DMOL package[51] was used, employing a double numeric plus polarization (DNP) basis along with an hexadecapole expansion to specify the maximum angular momentum function.[51]. The dielectric effect of the solvent was accounted for explicitly by the Conductor-like screening model (COSMO)[52]. For dots larger than $Si_{275}H_{172}$, the DFT calculations were performed using the SIESTA package[53] with norm-conserving Troullier-Martins pseudopotentials[54].

Brus *et al*. have proved that for sufficiently large quantum dots with radius R and dielectric constant ε_2 embedded in the environment with dielectric constant ε_1, the ionization potential (IP) and the electron affinity (EA) can be approximated by[55]

$$E(\varepsilon_1, \varepsilon_2, R) \approx \frac{\hbar^2 \pi^2}{2m^* R^2} + \frac{e^2}{2R} P'(\varepsilon_1, \varepsilon_2) + g(\varepsilon_1, \varepsilon_2), \quad (1)$$

where m^* is the effective mass of electron or hole. Small dots often have irregular shapes, and thus the number of Si atoms N is a preferable quantity to the radius as a measure of dot size, which has a close correlation to the solvent effect. Consequently, available data can be fit to the following equation,

$$E(\varepsilon_1, \varepsilon_2, N) - E(\varepsilon_0, \varepsilon_2, N) \approx f(\varepsilon_1, \varepsilon_2) N^{-1/3} + h(\varepsilon_1, \varepsilon_2), \quad (2)$$

where $E(\varepsilon_1, \varepsilon_0/\varepsilon_2, N)$ are the IP or EA of the dot with N atoms. P', g, f, h are functions of dielectric constant, while independent to the dot size. Once the values of $f(\varepsilon_1, \varepsilon_2)$ and $h(\varepsilon_1, \varepsilon_2)$ were determined, the solvent effect for large dots could be extrapolated.

The finite-difference method in real space with a norm-conserving pseudo potential, implemented in Parsec package,[56] was used to calculate absorption spectrum. The grid spacing was 0.25 Å, and the boundary radius was examined to ensure that the wave function vanished outside the sphere shell. Time-dependent DFT (TDDFT) calculations were subsequently carried out within the local adiabatic approximation (TDLDA)[57] as implemented in the RGWBS suite of codes.[58]

Without consideration of phonon-assistance, the photoluminescence (PL) rate at room temperature was calculated via Fermi's golden rule:[59,60]

$$k_{PL} = \sum_s p(s) \frac{4e^2 f_1^2(\varepsilon_{mol})\omega_s^3}{3c^3\hbar^3} \left| \vec{M}_s \right|^2, \quad (3)$$

Here $p(s)$ is the room-temperature Boltzmann occupation, M_s is the dipole matrix element between excitonic state s and the ground state computed using the MX code[61], and f_1 is the local field factor defined as[59,62]

$$f_1(x) = \frac{2l+1}{(\varepsilon_{dot}/\varepsilon_{sol}+1)l+1} = \frac{3}{\varepsilon_{dot}/\varepsilon_{sol}+2}. \quad (4)$$

In addition, ε_{dot} and ε_{sol} are the effective dielectric constants of the SiQD and the solvent, respectively. ε_{dot} was taken to be 1.3 for the 1.7 nm dot as obtained in a previous, accurate calculation,[59] while those for 2.6 and 3.1 nm dots were estimated to be 8.3 and 8.8 using the generalized Penn's model:[63]

$$\varepsilon_s(R) = 1 + \frac{\varepsilon_b - 1}{1 + (\alpha/R)^l}. \quad (5)$$

Here $\alpha = 6.9$ Å, and $l = 1.37$ Å.

To justify that our computational methodology does capture the essential factors to qualitatively predict the optical properties of SiQDs, we reproduced the substantial redshift of PL and absorption spectra observed in styryl (Phe) and (trimethylsilyl)vinyl (TMS) capped SiQDs with respect to the octyl (Oct) capped SiQDs.[21] In addition, our computed PL lifetimes agree reasonably well with previous experimental data[20,41,59,64-66]. Details on these checks, along with other relevant analyses, can be found in the Supporting Information.

Results and Discussion

A hydrogen passivated, 1.7 nm diameter SiQD ($Si_{147}H_{100}$) was analyzed under five conditions in order to elucidate our basic design premise. The absorption spectrum was calculated for the original dot and after modification with two types of molecules. As shown in Fig. 2 (right), 1-butene (C_4H_8) has a Type-I energy level alignment relative to the dot while 4-vinyl-N,N-bis(4-methoxyphenyl)aniline (MeO-TPA) offers a Type-II alignment. In the second case, the desired type-II energy level alignment was achieved by adding two methoxyl groups to triphenyl amine in order to raise the HOMO. Both molecules can be attached with either C-C or C=C connectivity, and absorption data was generated for each of these

four possibilities. A Type-I interface with the Si-C=C connections (Fig. 2(e)) only slightly increases absorption in the high-energy range and has a negligible influence in the low-energy range (Fig. 2(a)). In contrast, when a Type-II energy level alignment is formed with the Si-C-C connectivity, additional absorption peaks emerge inside the optical gap of the dot, but their intensities are very low due to the small overlap between the HOMO and the LUMO wave functions (Fig. 2(d)). Strong absorption in the low energy range occurs only when a Type-II interface is formed with the Si-C=C connections (Fig. 2(c))– i.e. both design rules need to be enforced. The generality of these rules is verified by similar observations on another ligand candidate $C_8H_{10}N_2S$ (Supporting Information, Fig. S14).

Optical properties were next considered as a function of dot diameter, d, with MeO-TPA functionalization. As quantified in Fig. 3(a), the transition from Type-II to Type-I alignment occurs at $d \approx 5.5$ nm, so MeO-TPA is a good prototypical functionalizer for this study. Moreover, the calculated absorption spectra of MeO-TPA-treated SiQDs show a strong absorption cross-section for $d = 1.7$, 2.6 and 3.1 nm, as summarized in Fig. 3(d-f). Although the redshift decreases with increasing dot size, the absorption intensity near the absorption edge is still significantly enhanced for even the largest dots.

The 2.6 nm SiQDs are in the middle of the range studied and are of a size that can be easily synthesized. Functionalization of them with four MeO-TPA ligands resulted in a 0.47 eV redshift of the optical gap (based on the PL peak), and a 0.94 eV redshift of the first strong absorption peak (Fig. 3(e)). The analysis shows that, while the peaks below 2 eV should be ascribed to the excitation from the HOMO of the MeO-TPA to a range of unoccupied orbitals of the dot, the peaks above 2 eV have three contributions: the spatially separated exciton; the intensified transition from deep occupied to unoccupied levels of the dot; and the excitation on the ligand itself (Fig. 3(b, c)).

Additional analysis of these 2.6 nm dots indicates that the absorption spectrum is not sensitive to the position and orientation of the MeO-TPAs and that the absorption strength peak increases with MeO-TPA coverage. (Supporting Information, Section II)

The calculated PL rates were found to increase remarkably with MeO-TPA functionalization for all dot sizes considered (Table 1). Although these rates are almost certainly underestimated due to the neglect of the phonon-assistance,[65] the trend is expected to be reasonable because of the large oscillator strength associated with the spatially separated exciton. Fortunately, such comparatively rapid PL will not affect energy conversion since it is still much slower than the subsequent charge separation and transport in the presence of a Type-II interface. Indeed, consistent with experiment,[11] our calculated charge separation rate is as high as 4.0×10^{12} s^{-1} in assemblies of perfect H-capped SiQDs blended with P3HT[67], only slightly decreasing to 2.3×10^{12} s^{-1} as a result of MeO-TPA

functionalization.

Table 1 PL lifetimes (seconds) of Si_{147}, Si_{465} and Si_{849} with only H-termination and with 4 MeO-TPA molecules.

	No MeO-TPA	With MeO-TPA
$Si_{147}H_{100}$	1.2×10^{-4}	6.5×10^{-6}
Si_{465}	1.1×10^{-3}	4.0×10^{-5}
Si_{849}	2.3×10^{-3}	1.4×10^{-4}

### Robustness with Respect to Contamination

The above results suggest that, in principle, MeO-TPA capping should significantly redshift the optical absorption of small SiQDs while also improving their absorption cross-section. To be useful in practice, though, these properties must be robust in the face of inevitable oxidation and the introduction of other types of ligands often added to improve processability.

The effect of oxidation was quantified by gradually increasing the coverage of oxidized backbonds from 0% to 74% at the outmost shell of Si_{465} both with and without four MeO-TPA ligands (Fig. 4(a)). As shown in Fig. 4(b), without MeO-TPA, the optical gap of the dot tends to decrease with increasing oxygen (O) density, consistent with previous calculations.[43–45] The fluctuations shown are due to a sensitivity to insertion sites. In contrast, the optical gap of MeO-TPA-capped dots at first goes down with increasing O density, dropping by as much as 0.3 eV, and then increases back to and even slightly above that of the unoxidized dots. This is because, regardless of the O level, the HOMO and LUMO are localized on the dot without MeO-TPA while they become localized on the MeO-TPA and dot separately when that ligand is added (Fig. 4(a)). Additional analysis is provided in the Supporting Information, where Figs. S5 and S6 summarize distinctive trends associated with frontier orbital localization. Without MeO-TPA, the HOMO spreads to the dot surface while the LUMO first expands and then shrinks into the core with increasing oxidation. With MeO-TPA, though, the HOMO and LUMO do not change significantly until two-thirds of the backbonds are oxidized.

Oxidation modifies not only the optical gap of the MeO-TPA-capped SiQD (up to 0.3 eV for the Si_{465} dot) but also the absorption spectrum. Fig. 4(c) shows that absorption intensity first increases until about 40% oxidation and then decreases with further severity of oxidation. When less than 40% surface backbonds are oxidized, the absorption of the MeO-TPA-capped SiQDs are much stronger than that of the dots without MeO-TPA, and that of the oxidized dots are much stronger than that of the oxygen-free dots, as demonstrated in 4(d). However, if the oxidation coverage is above 65%, the contribution of spatially separated exciton to the absorption will
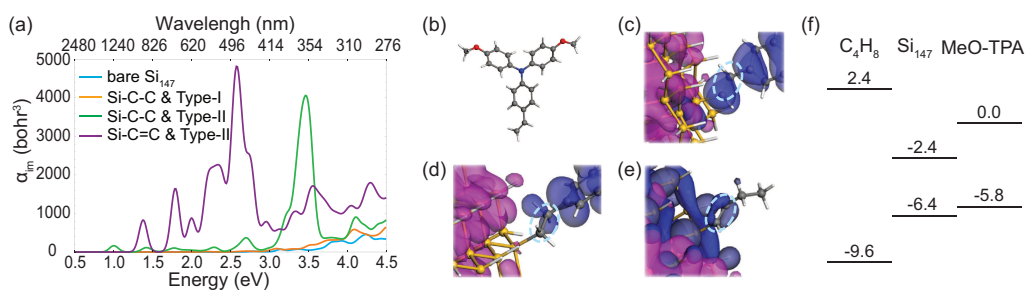
Fig. 2 (a) Calculated absorption spectra of bare Si_{147}, 4 MeO-TPA on Si_{147} with C=C connections, 4 MeO-TPA on Si_{147} with C-C connectivity and 4 C_4H_7 on Si_{147} with C=C connectivity. (b) Structure of the MeO-TPA molecule. The dot-ligand interfaces of Si_{147} capped by: (c) 4 MeO-TPA with C=C connectivity, (d) 4 MeO-TPA with C-C connectivity and (e) 4 1-butenes along with HOMO (blue) and LUMO (purple). The light blue ellipses highlight the relevant C=C and C-C bonds. The values of the isosurfaces are 0.007 $Å^{-3/2}$ in panel (c-e). (f) Energy level alignment between Si_{147}, C_4H_8 and MeO-TPA in eV.
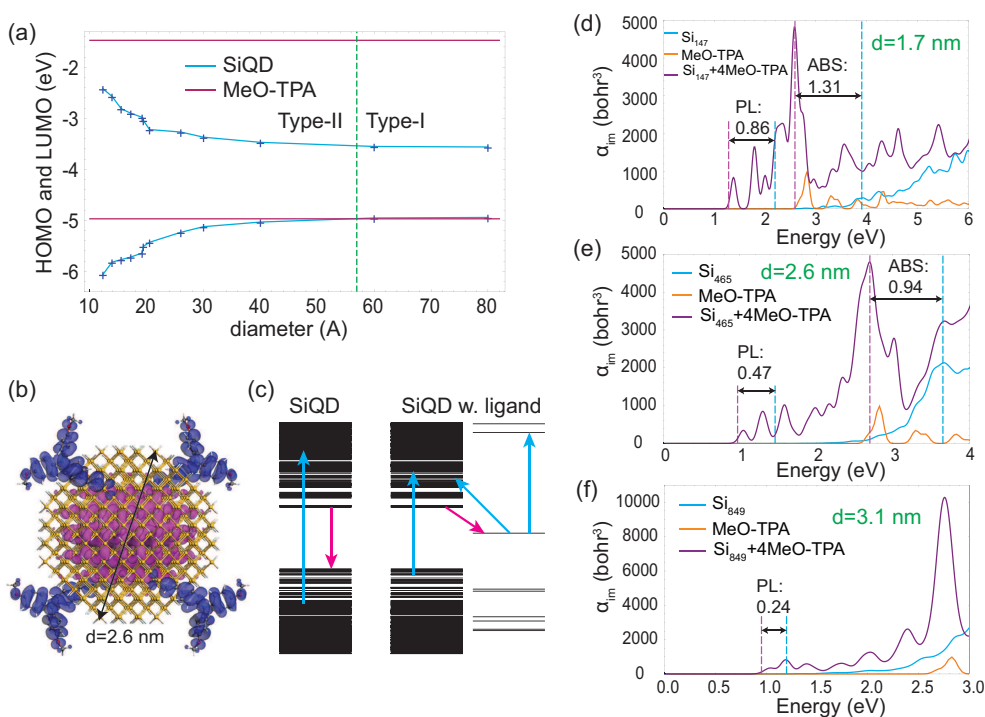
Fig. 3 (a) Energy level alignment between SiQDs of different sizes and MeO-TPA in dichloromethane solvent ($\varepsilon = 9.08$). The dashed green line denotes the transition from a Type-II to a Type-I interface. (b) HOMO (blue) and LUMO (purple) of Si_{465} capped by 4 MeO-TPA ligands. Isosurfaces are 0.009 $Å^{-3/2}$. (c) Illustration of absorption (upward blue arrows) and emission (downward red arrows) on H-passivated and MeO-TPA-functionalized dots. Comparison of the influences of MeO-TPA ligand on absorption spectra of SiQD with different sizes from (d) Si_{147} (1.7 nm) to (e) Si_{465} (2.6 nm) to (f) Si_{849} (3.1 nm). The predicted redshift of photoluminescence (PL) and absorption (ABS) peaks are shown in unit of eV.
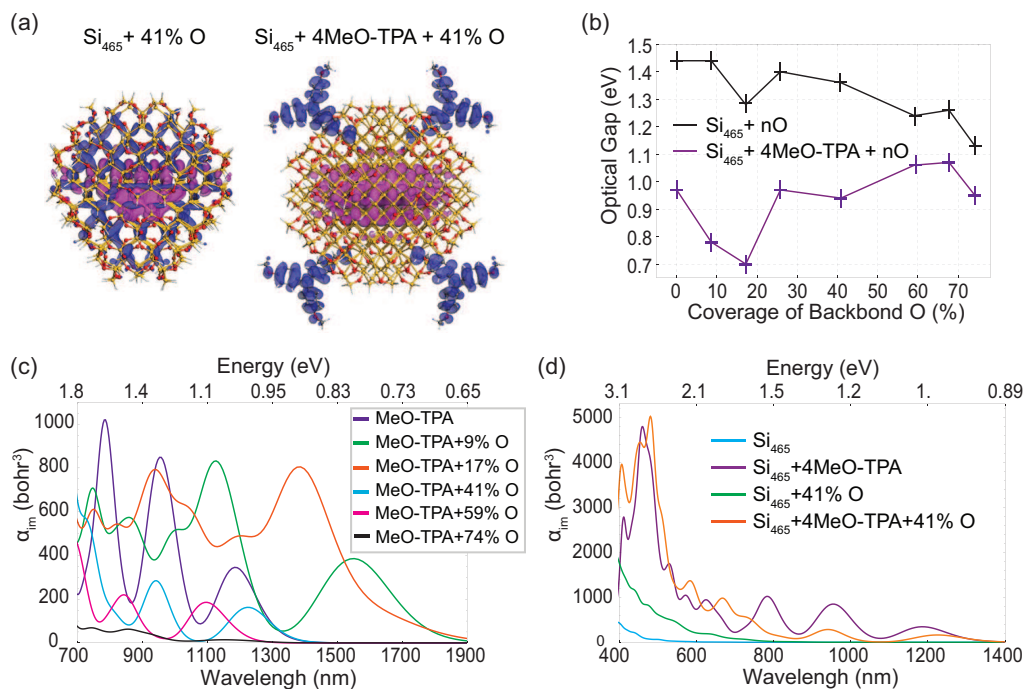
Fig. 4 (a) HOMO (blue) and LUMO (purple) isosurfaces of Si_{465} with 41% of surface backbonds oxidized without (left) and with (right) MeO-TPA. Isosurfaces are 0.009 Å$^{-3/2}$. (b) The optical gaps of H-passivated Si_{465} and MeO-TPA-functionalized Si_{465} with surface backbond oxidation ranging from 0% to 74%. (c) Absorption spectra of MeO-TPA-functionalized Si_{465} for several oxidation levels. (d) Absorption spectra of MeO-TPA-functionalized Si_{465} with 41% backbond oxidation compared to that without the MeO-TPA and that without oxygen.

be mostly quenched. Such tolerance of the optical properties to oxidation should allow experimental verification of the efficacy of MeO-TPA functionalization under realistic laboratory environments.

In regard to the charge dynamics, we find that oxidation changes the PL lifetime significantly, consistent with previous experimental work,[68] and its impact fluctuates with defect density due to wavefunction localization. Take the 1.7 nm SiQD as an example. While the PL lifetime decreases by a factor of 3.2, with 12% backbond sites oxidized, the lifetime increases by a factor of 2.5 when the defect density increases to 60%. The above influence, though, is not expected to affect the charge separation rate which is typically much higher.

Another type of contamination is alkyl chains, which are typically added to improve the solubility of dots. It has been reported that these ligands cause very little change in optical properties of the dot (near the absorption/emission edges) irrespective of chain length and ligand density, although HOMO and LUMO levels of the capped dots are shifted upward significantly.[39–41] For the MeO-TPA-capped dots, though, the alkyl chains could change the absorption near edge more significantly because the gap of the spatially separated exciton relies on the LUMO of the dot and the HOMO of the MeO-TPA, and the latter is nearly fixed. Our calculations suggest that, with

50% of the surface covered with methyl, the increase of the near-edge absorption intensity relative to that of H-terminated dots is preserved. However, a reduction in the optical gap attributed to the MeO-TPA ligand is totally offset by the increase of the LUMO level due to the presence of methyl (Supporting Information, Fig. S7). Because of this, the alkyl termination should be minimized or replaced by other functional groups.

Conclusions

The optical properties of small silicon quantum dots can be significantly red-shifted through the use of carefully chosen organic ligands. This has the potential to solve a long-running problem associated with small SiQDs–that their optical gaps are too high for many technological applications. A design strategy was proposed with two criteria: (1) a Type-II energy level alignment must exist between dot and functionalizing ligand; and (2) conjugating vinyl bond connectivity needs to be created between the dot and ligand to enhance the absorption cross-section. In concert with the traditional method of tuning optical gaps using the relationship between quantum confinement and dot size, the new strategy allows an additional degree of design freedom to exploit the novel properties of small SiQDs.

A proof-of-concept was established for a prototype system consisting of a 2.6 nm SiQD functionalized by MeO-TPA ligands. The result was a 0.47 eV redshift in optical gap along with a substantial enhancement of the absorption intensity near the edge.

While strong absorption has been previously achieved by Type-II core-shell quantum dots, it is difficult to move carriers localized within the cores out to electrodes. The proposed functionalization scheme could solve this problem, because the sparse ligand layer allows dots to be connected using bridging molecules so as to enhance the electron coupling between adjacent dots.[69]

Acknowledgement

References

1 K. Y. Cheng, R. Anthony, U. R. Kortshagen and R. J. Holmes, *Nano Lett.*, 2011, **11**, 1952–1956.

2 N. Daldosso and L. Pavesi, *Laser & Photonics Reviews*, 2009, **3**, 508–534.

3 H. W. Hillhouse and M. C. Beard, *Curr. Opin. Colloid Interface Sci.*, 2009, **14**, 245–259.

4 J. Liu, F. Erogbogbo, K.-T. Yong, L. Ye, J. Liu, R. Hu, H. Chen, Y. Hu, Y. Yang, J. Yang, I. Roy, N. A. Karker, M. T. Swihart and P. N. Prasad, *ACS Nano*, 2013, **7**, 7303–7310.

5 F. Peng, Y. Su, Y. Zhong, C. Fan, S.-T. Lee and Y. He, *Acc. Chem. Res.*, 2014, **47**, 612–623.

6 N. Tomczak, R. R. Liu and J. G. Vancso, *Nanoscale*, 2013, **5**, 12018–12032.

7 M. C. Beard, K. P. Knutsen, P. R. Yu, J. M. Luther, Q. Song, W. K. Metzger, R. J. Ellingson and A. J. Nozik, *Nano Lett.*, 2007, **7**, 2506–2512.

8 A. Pandey and P. Guyot-Sionnest, *Science*, 2008, **322**, 929–932.

9 D. Talapin and J. Lee, *Chem. Rev.*, 2010, **110**, 389–458.

10 C. M. Hessel, D. Reid, M. G. Panthani, M. R. Rasch, B. W. Goodfellow, J. W. Wei, H. Fujii, V. Akhavan and B. A. Korgel, *Chem. Mater.*, 2012, **24**, 393–401.

11 D. Herrmann, S. Niesar, C. Scharsich, A. Koehler, M. Stutzmann and E. Riedle, *J. Am. Chem. Soc.*, 2011, **133**, 18220–18233.

12 J.-W. Luo, P. Stradins and A. Zunger, *Energy Environ. Sci.*, 2011, **4**, 2546–2557.

13 S. Niesar, W. Fabian, H. Petermann, Nils, R. Daniel, W. Eberhard, M. Hartmut, Brandt and S. Martin, *Green*, 2011, **1**, 339–350.

14 C.-Y. Liu, Z. C. Holman and U. R. Kortshagen, *Nano Lett.*, 2009, **9**, 449–452.

15 C.-Y. Liu, Z. C. Holman and U. R. Kortshagen, *Adv. Funct. Mater.*, 2010, **20**, 2157–2164.

16 E.-C. Cho, S. Park, X. Hao, D. Song, G. Conibeer, S.-C. Park and M. A. Green, *Nanotechnology*, 2008, **19**, year.

17 G. Conibeer, M. Green, E.-C. Cho, D. Koenig, Y.-H. Cho, T. Fangsuwannarak, G. Scardera, E. Pink, Y. Huang, T. Puzzer, S. Huang, D. Song, C. Flynn, S. Park, X. Hao and D. Mansfield, *Thin Solid Films*, 2008, **516**, 6748–6756.

18 X. J. Hao, E. C. Cho, G. Scarder, Y. S. Shen, E. Bellet-Amalric, D. Bellet, G. Conibeer and M. A. Green, *Sol. Energ. Mat. Sol.* , 2009, **93**, 1524–1530.

19 S. Niesar, R. N. Pereira, A. R. Stegner, N. Erhard, M. Hoeb, A. Baumer, H. Wiggers, M. S. Brandt and M. Stutzmann, *Adv. Funct. Mater.*, 2012, **22**, 1190–1198.

20 D. C. Hannah, J. Yang, P. Podsiadlo, M. K. Chan, A. Demortiere, D. J. Gosztola, V. B. Prakapenka, G. C. Schatz, U. Kortshagen and R. D. Schaller, *Nano Lett.*, 2012, **12**, 4200–4205.

21 M. X. Dung, D. D. Tung, S. Jeong and H.-D. Jeong, *Chem. Asian J.*, 2013, **8**, 653–664.

22 C.-C. Lin, M.-H. Tan, C.-P. Tsai, K.-Y. Chuang and T. Lay, *IEEE J. Sel. Top. Quant. Electron.*, 2013, **19**, 1–10.

23 H. Li, M. T. Lusk, R. T. Collins and Z. Wu, *ACS Nano*, 2012, **6**, 9690–9699.

24 M. C. Beard, A. G. Midgett, M. C. Hanna, J. M. Luther, B. K. Hughes and A. J. Nozik, *Nano Lett.*, 2010, **10**, 3019–3027.

25 A. J. Nozik, M. C. Beard, J. M. Luther, J. C. Johnson, O. E. Tavi, A. G. Midgett, M. C. Hanna and B. K. Hughes, *Abstr. Pap. Am. Chem. S.*, 2011, **242**, year.

26 P. Wörfel, *Physics of Solar cells: from Principles to new Concepts*, WILEY-VCH Verlag, 2005.

27 A. Gupta, M. T. Swihart and H. Wiggers, *Adv. Funct. Mater.*, 2009, **19**, 696–703.

28 A. Shiohara, S. Hanada, S. Prabakar, K. Fujioka, T. H. Lim, K. Yamamoto, P. T. Northcote and R. D. Tilley, *J. Am. Chem. Soc.*, 2010, **132**, 248–253.

29 M. Rosso-vasic, E. Spruijt, Z. Popovi, K. Overgaag, B. V. Lagen, B. Grandidier, D. Vanmaekelbergh and D. Dominguez, *J. Mater. Chem.*, 2009, **19**, 5926–5933.

30 T. M. Atkins, A. Thibert, D. S. Larsen, S. Dey, N. D. Browning and S. M. Kauzlarich, *J. Am. Chem. Soc.*, 2011, **133**, 20664–20667.

31 J. H. Warner, A. Hoshino, K. Yamamoto and R. D. Tilley, *Angew. Chem.*, 2005, **117**, 4626–4630.

32 J. H. Warner, H. Rubinsztein-Dunlop and R. D. Tilley, *J. Phys. Chem. B*, 2005, **109**, 19064–19067.

33 G.-R. Lin, C.-J. Lin, C.-K. Lin, L.-J. Chou and Y.-L. Chueh, *J. Appl. Phys.*, 2005, **97**, 094306.

34 C.-J. Lin and G.-R. Lin, *IEEE J. Sel. Top. Quant. Electron.*, 2005, **41**, 441–447.

35 I. Umezu, A. Sugimura, T. Makino, M. Inada and K. Matsumoto, *J. Appl. Phys.*, 2008, **103**, 024305–024305.

36 M. V. Wolkin, J. Jorne, P. M. Fauchet, G. Allan and C. Delerue, *Phys. Rev. Lett.*, 1999, **82**, 197–200.

37 B. Ghosh and N. Shirahata, *Sci. Tech. Adv. Mater.*, 2014, **15**, year.

38 L. E. Brus, *J. Chem. Phys*, 1984, **80**, 4403–4409.

39 F. A. Reboredo and G. Galli, *J. Phys. Chem. B*, 2005, **109**, 1072–1078.

40 A. Gali, M. Voros, D. Rocca, G. T. Zimanyi and G. Galli, *Nano Lett.*, 2009, **9**, 3780–3785.

41 R. Wang, X. Pi and D. Yang, *J. Phys. Chem. C*, 2012, **116**, 19434–19443.

42 R. Wang, X. Pi and D. Yang, *Phys.Chem. Chem. Phys.*, 2013, **15**, 1815–1820.

43 Z. Zhou, R. A. Friesner and L. Brus, *J. Am. Chem. Soc.*, 2003, **125**, 15599–15607.

44 R. J. Eyre, J. P. Goss and P. R. Briddon, *Phys. Rev. B*, 2008, **77**, 245407.

45 C. S. Garoufalis and A. D. Zdetsis, *Phys. Chem. Chem. Phys.*, 2006, **8**,

808–813.

46 Q. S. Li, R. Q. Zhang, S. T. Lee, T. A. Niehaus and T. Frauenheim, *Appl. Phys. Lett.*, 2008, **92**, 053107.

47 S. A. Ivanov, A. Piryatinski, J. Nanda, S. Tretiak, K. R. Zavadil, W. O. Wallace, D. Werder and V. I. Klimov, *J. Am. Chem. Soc.*, 2007, **129**, 11708–11719.

48 H. Zhu, N. Song and T. Lian, *J. Am. Chem. Soc.*, 2011, **133**, 8762–71.

49 L. P. Balet, S. A. Ivanov, A. Piryatinski, M. Achermann and V. I. Klimov, *Nano Lett.*, 2004, **4**, 1485.

50 J. P. Perdew and Y. Wang, *Phys. Rev. B*, 1992, **45**, 13244–13249.

51 B. Delley, *J. Chem. Phys.*, 1990, **92**, 508–517.

52 A. Klamt, V. Jonas, T. Burger and J. C. W. Lohrenz, *J. Phys. Chem. A*, 1998, **102**, 5074–5085.

53 J. Soler, E. Artacho, J. Gale, A. Garcia, J. Junquera, P. Ordejon and D. Sanchez-Portal, *J. Phys.: Condens. Matter*, 2002, **14**, 2745–2779.

54 N. Troullier and J. L. Martins, *Phys. Rev. B*, 1991, **43**, 8861–8869.

55 L. BRUS, *J. Chem. Phys*, 1983, **79**, 5566–5571.

56 J. R. Chelikowsky, *Phys. Rev. Lett.*, 1994, **72**, 1240–1243.

57 M. Rohlfing and S. G. Louie, *Phys. Rev. B*, 2000, **62**, 4927–4944.

58 M. L. Tiago and J. R. Chelikowsky, *Phys. Rev. B*, 2006, **73**, 205334.

59 Z. Lin, H. Li, A. Franceschetti and M. T. Lusk, *ACS Nano*, 2012, **6**, 4029–4038.

60 M. Califano, A. Franceschetti and A. Zunger, *Nano Lett.*, 2005, **5**, 2360–2364.

61 A. Franceschetti, H. Fu, L. W. Wang and A. Zunger, *Phys. Rev. B*, 1999, **60**, 1819–1829.

62 R. Baer and E. Rabani, *J. Chem. Phys*, 2008, **128**, year.

63 L.-W. Wang and A. Zunger, *Phys. Rev. Lett.*, 1994, **73**, 1039–1042.

64 A. Puzder, A. J. Williamson, F. A. Reboredo and G. Galli, *Phys. Rev. Lett.*, 2003, **91**, 157405.

65 C. Delerue, G. Allan and M. Lannoo, *Phys. Rev. B*, 2001, **64**, 193402.

66 M. L. Mastronardi, F. Maier-Flaig, D. Faulkner, E. J. Henderson, C. Kubel, U. Lemmer and G. A. Ozin, *Nano Lett.*, 2012, **12**, 337–342.

67 H. Li, Z. Wu and M. T. Lusk, *J. Phys. Chem. C*, 2014, **118**, 46–53.

68 G.-R. Lin, C.-J. Lin and K.-C. Yu, *J. Appl. Phys.*, 2004, **96**, year.

69 H. Li, Z. Wu, T. Zhou, A. Sellinger and M. T. Lusk, *Energy Environ. Sci.*, 2014, **7**, 1023–1028.